

Six-week time series of eddy covariance CO₂ flux at Mammoth Mountain,
California: performance evaluation and role of meteorological forcing

J.L. Lewicki^{a*}, M.L. Fischer^b, G.E. Hilley^c

^{a*}*Earth Sciences Division, Ernest Orlando Lawrence Berkeley National Laboratory, Berkeley,
CA, USA 94720, e-mail: jllewicki@lbl.gov, ph: 510-495-2818, fax: 510-486-5686*

^b*Environmental Energy Technology Division, Ernest Orlando Lawrence Berkeley National
Laboratory, Berkeley, CA, USA 94720, e-mail: mlfischer@lbl.gov*

^c*Department of Geological and Environmental Sciences, Stanford University, Stanford, CA, USA
94305, e-mail: hilley@pangea.stanford.edu*

Abstract

CO₂ and heat fluxes were measured over a six-week period (09/08/2006 to 10/24/2006) by the eddy covariance (EC) technique at the Horseshoe Lake tree kill (HLTK), Mammoth Mountain, CA, a site with complex terrain and high, spatially heterogeneous CO₂ emission rates. EC CO₂ fluxes ranged from 218 to 3500 g m⁻² d⁻¹ (mean = 1346 g m⁻² d⁻¹). Using footprint modeling, EC CO₂ fluxes were compared to CO₂ fluxes measured by the chamber method on a grid repeatedly over a 10-day period. Half-hour EC CO₂ fluxes were moderately correlated ($R^2 = 0.42$) with chamber fluxes, whereas average-daily EC CO₂ fluxes were well correlated ($R^2 = 0.70$) with chamber measurements. Average daily EC CO₂ fluxes were correlated with both average daily wind speed and atmospheric pressure; relationships were similar to those observed between chamber CO₂ fluxes and the atmospheric parameters over a comparable time period. Energy balance closure was assessed by statistical regression of EC energy fluxes (sensible and latent heat) against available energy (net radiation, less soil heat flux). While incomplete ($R^2 = 0.77$ for 1:1 line), the degree of energy balance closure fell within the range observed in many investigations conducted in contrasting ecosystems and climates. Results indicate that despite complexities presented by the HLTK, EC can be reliably used to monitor background variations in volcanic CO₂ fluxes associated with meteorological forcing, and presumably changes related to deeply derived processes such as volcanic activity.

Keywords: CO₂ emissions; volcano monitoring; eddy covariance; chamber method;
Mammoth Mountain

1. Introduction

The measurement of surface emissions of CO₂ has become an integral part of many volcanic and geothermal monitoring programs, as temporal variations in emissions may indicate changes at depth associated with volcanic activity or geothermal processes (e.g., Baubron et al., 1991; Farrar et al., 1995; Chiodini et al., 1998; Hernandez et al., 1998; Klusman et al., 2000; McGee et al., 2000; Bergfeld et al., 2001; Hernandez et al., 2001; Werner and Cardellini, 2006). Furthermore, it is important to understand the link between temporal variations in deeply derived CO₂ emissions, and meteorologic and hydrologic processes, as these near-surface processes can drive large changes in CO₂ emissions (e.g., Connor et al., 1993; McGee and Gerlach, 1998; Rogie et al., 2001; Granieri et al., 2003; Lewicki et al., 2007) that may pose health and environmental hazards or be misinterpreted to reflect changes at depth.

While the chamber method (e.g., Chiodini et al., 1998) has been reliably used to measure spatial and temporal variations in surface CO₂ fluxes in many volcanic and geothermal regions, limitations of the method include the measurement's small spatial scale (<1 m²), alteration of the ground surface and gas flow during the measurement, and the ability to continuously monitor temporal changes in CO₂ fluxes at only a single or limited number

of point locations within a study area. The eddy covariance (EC) method, a micrometeorological technique traditionally used to measure CO₂ (and other trace gas and heat) fluxes across the interface between the atmosphere and a plant canopy (e.g., Baldocchi, 2003 and references therein) has been proposed as a viable and complementary technique to monitor volcanic CO₂ and heat fluxes in conjunction with the chamber method (Werner et al., 2000; 2003; 2006; Anderson and Farrar, 2001). EC provides the benefit of an automated flux measurement that does not interfere with the ground surface and is averaged over both time and space, with the spatial scale significantly larger (m²-km²) than that of the chamber method. Importantly, however, the theory that underlies the EC method assumes spatial homogeneity of surface fluxes, flat terrain, and temporal stationarity (e.g., Folken and Wichura, 1996), conditions that are not typically met in volcanic and geothermal environments.

Work in mountain ecosystems has shown that under suitable atmospheric conditions, EC can provide reliable CO₂ and heat flux measurements in complex terrain (e.g., Turnipseed et al., 2003; 2004). Werner et al. (2000; 2003) deployed EC from 1 to 2.5 weeks in the Yellowstone National Park hydrothermal system, USA and at Solfatara volcano, Italy, sites with highly heterogeneous surface CO₂ and heat fluxes, yet relatively flat terrain. Using footprint modeling, they showed general consistency between EC CO₂ fluxes and chamber CO₂ fluxes measured on grids, indicating that EC yielded representative measurements at these sites. However, Werner et al. (2003) suggested that the relative difference observed between the two methods could have been derived in part by incomplete characterization of the temporal variability of surface CO₂ fluxes within the

study area by the chamber method over the EC measurement period. Anderson and Farrar (2001) performed EC measurements of CO₂ and heat fluxes for up to four days in three pilot studies at the Horseshoe Lake tree kill (HLTK) on Mammoth Mountain, USA (Figure 1). The HLTK is a site with complex terrain and highly heterogeneous, yet cold volcanic CO₂ emissions, thus possessing distinctly different characteristics from the Yellowstone and Solfatara areas. While they found average EC CO₂ flux measurements to be generally similar to chamber measurements made in separate studies, footprint modeling as performed by Werner et al. (2000; 2003) would have been required to directly compare the results derived from these two methods.

We build on the work of Werner et al. (2000; 2003) and Anderson and Farrar (2001) by presenting a six-week time series of EC CO₂ fluxes measured at the HLTK. We assess the quality of EC CO₂ and heat flux measurements by comparing them to measurements made by independent techniques. In particular, EC CO₂ fluxes were compared to chamber CO₂ fluxes over a 10-day period when spatio-temporal variations in surface CO₂ fluxes were captured by repeated chamber measurements on a grid. Despite the complexities presented by the study site, we show that under certain atmospheric conditions, the EC method performs well relative to independent methods. Finally, the multi-week time series of EC fluxes allowed us to establish relationships between temporal variations in surface CO₂ fluxes and meteorological parameters on time scales longer than a day.

2. Study Site

Mammoth Mountain (3368 m) is a dormant dacitic volcano formed 200,000 to 50,000 years ago on the southwestern rim of Long Valley caldera, eastern California (Figure 1). While lavas were last erupted ~50,000 years ago, phreatic eruptions occurred up to ~700 years ago (Bailey, 1989). Recent volcanic unrest associated with Mammoth Mountain was first detected in 1979 and activity was subsequently expressed as ground deformation, swarms of small earthquakes ($M \leq 3$), spasmodic bursts, long-period and very long-period earthquakes, elevated $^3\text{He}/^4\text{He}$ ratios in fumarolic gases, and diffuse surface CO_2 emissions (Hill and Prejean, 2005). An eleven-month-long seismic swarm occurred at Mammoth Mountain in 1989, possibly related to dike intrusion and/or magmatic fluid migration (Hill, 1996; Hill and Prejean, 2005). Tree kills then formed in six general areas on Mammoth Mountain in 1990-1991 due to diffuse, non-thermal emissions of volcanic CO_2 resulting in high CO_2 concentrations in the root zone (e.g., Farrar et al., 1995).

The HLTK is the largest ($\sim 120,000 \text{ m}^2$) tree kill on Mammoth Mountain and is located on the northwest shore of Horseshoe Lake, on the southeast flank of the volcano (Figure 1). It lies in the Lakes Basin, with terrain sloping upward to the west-northwest (Figures 1 and 2). Soils here are largely barren of vegetation, 1 to 3 m thick, and composed of 0.1 to 0.4 m of pumice overlying coarse sand with cobbles to boulders and low organic carbon (McGee and Gerlach, 1998; Evans et al., 2001). Horseshoe Lake is perched, while the water table here is located at ~40 m depth (HSL-1 well; Farrar et al., 1998).

Extensive monitoring of subsurface CO₂ concentrations and surface CO₂ fluxes has been conducted at the HLTK (e.g., Farrar et al., 1995; Rahn et al., 1996; Gerlach et al., 1998; McGee and Gerlach, 1998; McGee et al., 2000; Gerlach et al., 2001; Anderson and Farrar, 2001; Rogie et al., 2001; Lewicki et al., 2007). Studies have reported large diurnal to seasonal fluctuations in time series of soil CO₂ concentrations, surface CO₂ fluxes, and total CO₂ discharges that appear to be due to variations in meteorological and hydrologic processes (e.g., McGee and Gerlach, 1998; McGee et al., 2000; Rogie et al., 2001). Also, Lewicki et al., (2007) showed that large spatio-temporal variations in surface CO₂ fluxes over multiple days can be driven by slow-moving cold fronts. Furthermore, long-term monitoring suggests that emissions have markedly declined over the past decade. For example, the average estimated CO₂ discharge from the tree kill area was ~250 t d⁻¹ for 1995 to 1997 (Gerlach et al., 1998) and 93 t d⁻¹ for 1997 to 2000 (Rogie et al., 2001), whereas the average discharge measured in 2006 was 38 t d⁻¹ (Lewicki et al., 2007).

3. Methods

3.1. Eddy covariance measurements

An EC station (2.5 m high; see below) was deployed at the HLTK (Figure 2) continuously from 09/08/2006 to 10/24/2006. The location of the station was chosen to take advantage of the westerly prevailing winds and the absence of asphalt road and parking lot to the west. The average surface slope to the west (from directions of 190 to

360°) and within 100 m of the station was 9% (range = 1 to 15%; Figure 2). Within 300 m of the station, the average slope was 13% (range = 1 to 18%). Widely distributed tree stumps, rocks, and logs were located within about 50 m of the EC station. In addition, foliage-free standing dead trees, which have lost the majority of fine branches, were located from about 50 to 200 m from the EC station (Figure 1).

The EC station was similar in design to that described by Billesbach et al. (2004) and was composed of fast-response and slow-response subsystems. The fast-response subsystem included two sensors used to measure the variables necessary to calculate turbulent fluxes of CO₂, H₂O, heat, and momentum. A Gill-Solent WindMaster Pro sonic three-dimensional anemometer/thermometer (Gill Instruments, Ltd) measured wind speeds in three directions and sonic temperature at 10 Hz. A LI-COR 7500 open-path CO₂-H₂O infrared gas analyzer (LI-COR, Inc) measured CO₂ and water vapor densities at 10 Hz. Both sensors were mounted to the top of a tripod tower at 2.5 m height.

The slow-response subsystem included sensors associated with a second tripod tower that measured auxiliary variables used to compare with EC fluxes and establish relationships between EC fluxes and environmental parameters. Atmospheric pressure was measured using a Vaisala PTB101B barometer (Vaisala, Inc.). Atmospheric temperature and relative humidity were measured using a Vaisala HMP50 humidity and temperature probe. Mean horizontal wind speed and direction were measured by a Climatronics CS800-12 wind set (Climatronics Corp.) at 2.5 m height. Net radiation, total insolation and photosynthetically active radiation (PAR) were measured with a Kipp & Zonen

CNR-1 radiometer (Kipp & Zonen), LI-COR LI-200SA pyranometer, and LI-COR LI-190SA quantum sensor, respectively, mounted to a horizontal bar extending from the tripod tower at 2 m height. Mean precipitation was measured by a TE525 tipping bucket rain gage (Texas Electronics). Soil moisture profiles (10 and 30 cm depth) were measured at two locations using ECH2O (Decagon Devices) soil moisture probes. Soil temperature profiles (10, 20, and 30 cm depth) were measured at two locations with thermocouples. Soil heat flux was measured by four HFT3 soil heat flux plates (Radiation and Energy Balance Systems) located at 5 cm depth near the radiometer. Slow-response subsystem variables were measured every 5 seconds and averaged over 30 minutes for comparison with turbulent fluxes.

Carbon dioxide, latent heat (LE), sensible heat (H), and momentum fluxes (F_s) were calculated as the temporal covariance of the scalar (s) and vertical wind velocity (w):

$$F_s = \overline{w's'} \quad (1)$$

where the overbar denotes time averaging and primes denote deviations from a mean. Fluxes were calculated for 30-minute periods. Equation 1 gives the mean vertical turbulent flux of the scalar of interest over a horizontally homogeneous surface under steady-state conditions. Details on the theory and assumptions of the EC method can be found in Baldocchi et al. (1988); Foken and Wichura (1996); Aubinet et al. (2000); Baldocchi (2003).

For each half-hour of data, the mean lateral (\bar{v}) and then the mean vertical (\bar{w}) wind velocities were rotated to zero (Kaimal and Finnigan, 1994). The Webb correction for the effects of fluctuation in heat and water vapor on the density of air (Webb et al., 1980) was applied. Raw signals from the infrared gas analyzer and sonic anemometer were evaluated for voltage spikes and all points more than ten standard deviations (thereby accepting a non-Gaussian tail to the data) away from a 60 s moving average were removed from the data. Turbulent fluxes measured during periods of insufficient turbulent mixing are typically underestimated. To filter data for this effect, friction velocities (u_*) were calculated as the square root of the momentum flux. Figure 3 shows a plot of EC CO₂ flux versus u_* for all EC measurements corresponding to mean wind directions from 190 to 360° (i.e., hereafter, only EC measurements corresponding to mean wind directions from the tree kill area will be considered). EC CO₂ fluxes increase sharply with u_* until $u_* \sim 0.25 \text{ m s}^{-1}$, above which EC fluxes remain relatively constant (Figure 3). We eliminated all EC (CO₂ and heat) fluxes corresponding to $u_* \leq 0.25 \text{ m s}^{-1}$. A test for stationarity was conducted according to Foken and Wichura (1995). Each 30-minute EC flux measurement was divided into six five-minute segments. If the difference between the average of the six five minute segments and the 30-minute measurement was greater than 30%, the measurement was considered non-stationary and discarded. Specific details of data filtering are also shown on each of the following figures.

3.2. Chamber measurements

Surface CO₂ flux was measured using a WEST Systems fluxmeter (WEST Systems) based on the chamber method, with repeatability of $\pm 10\%$ (Chiodini et al., 1998). Evans et al. (2001) conducted laboratory measurements of imposed CO₂ fluxes over a range typical of Mammoth Mountain tree kill areas through a synthetic “soil” similar in properties to surficial deposits in the tree kill areas, and showed that chamber measurements were negatively biased, on average by 12.5%. Collars were not used for chamber measurements, due to due to the potential alteration of soil properties and gas flow (e.g., Gerlach et al., 2001). Surface CO₂ flux was measured at 170 grid points at 27-m spacing in the HLTK (Figure 2). Flux measurements were repeated in the same order along the grid each day from 09/12/2006 to 09/21/2006 between 07:00 and 15:00, with the exception of 09/15/2006 when no measurements were made. For the purpose of comparison with EC CO₂ fluxes, the negative bias in chamber measurements was corrected for by increasing each flux measurement by 12.5%. A map of surface CO₂ flux was then produced for each day of grid measurements using nearest neighbor interpolation at 5 x 5 m resolution, chosen for its simplicity in the comparison of chamber to EC CO₂ flux measurements. Surface CO₂ flux maps produced using the sequential Gaussian simulation method and corresponding total CO₂ discharges from the study area are presented in Lewicki et al. (2007). For reference, Lewicki et al. (2005) presented a comparison of a range of geostatistical interpolation and simulation methods that were applied to chamber CO₂ fluxes measured in a volcanic environment.

4. Results

4.1. Meteorology

Atmospheric temperatures ranged from -8.3 to 20.8°C and winds were dominantly from the west (Figure 4) over the study period. The highest wind speeds were measured from westerly directions, while easterly winds typically corresponded to relatively low wind speeds (Figure 4). Precipitation (typically light snow) occurred on six days during October (10/01/2006, 10/02/2006, 10/10/2006, 10/11/2006, 10/14/2006, and 10/17/2006) (Figures 5b and 7). Average daily wind speeds and atmospheric pressures varied from 1.1 to 3.5 m s^{-1} and 725 to 740 mbar , respectively from 09/08/2006 to 10/24/2006 (Figure 5a). A cold front occurred on 09/14/2006 to 09/15/2006 (Lewicki et al., 2007) and was accompanied by high average daily wind speeds and low atmospheric pressures (see zone I on Figure 5a). Over the entire measurement period (09/08/2006 to 10/24/2006), average daily wind speeds and atmospheric pressures were moderately inversely correlated (correlation coefficient = -0.43). From 09/08/2006 to 09/22/2006 (zone I, Figure 5a), average daily wind speed and pressure were strongly inversely correlated (correlation coefficient = -0.80). Relationships between meteorological parameters and chamber CO_2 fluxes over this time period were examined in Lewicki et al. (2007). We therefore selected this time frame to analyze relationships between meteorological parameters and EC CO_2 fluxes for comparison. From 09/24/2006 to 10/10/2006 (zone II, Figure 5a), average daily wind speed and pressure were poorly correlated (correlation coefficient = 0.14). We selected zone II to examine correlations between average daily wind speed, pressure, and EC CO_2 fluxes because of different meteorological conditions

(i.e., lack of a cold front) from zone I, and a sufficient number of EC data to perform the analysis.

4.2. Chamber fluxes

Large spatio-temporal variations in surface CO₂ fluxes were measured using the chamber method from 09/12/2006 to 09/21/2006 (Figures 5b and 6). During the first two days of measurements (09/12/2006 and 09/13/2006), the spatial distribution of surface CO₂ fluxes remained relatively stable (Figure 6a-b). Then, on 09/14/2006 surface CO₂ fluxes decreased and the region of relatively high flux began to contract in size (Figures 5b and 6c). On 09/16/2006, surface CO₂ fluxes continued to decrease and the region of elevated flux further contracted in size (Figures 5b and 6d). CO₂ fluxes then increased and the region of elevated CO₂ flux expanded outwards on 09/17/2006 to 09/18/2006 (Figures 5b and 6e-f). With the exception of on 09/19/2006, surface CO₂ fluxes continued to increase over the remainder of the measurement period (Figures 5b and 6g-i). Further details on the spatio-temporal variations in chamber CO₂ fluxes are found in Lewicki et al. (2007).

4.3. Eddy covariance CO₂ fluxes

EC CO₂ fluxes measured from 09/08/2006 to 10/24/2006 ranged from 218 to 3500 g m⁻² d⁻¹ (Figure 7), with a mean and standard deviation of 1346 and 575 g m⁻² d⁻¹, respectively. Large gaps in the time series of CO₂ fluxes were present due to filtering for mean horizontal wind direction, u_* , and stationarity. For example, 47% of the EC CO₂

fluxes corresponding to wind directions from 190 to 360° were lost due to filtering for u_* and stationarity.

4.4. Comparison of eddy covariance to chamber CO₂ fluxes

The vertical scalar flux (e.g., of CO₂; F_{CO_2}) measured by EC at point (x_m, y_m, z_m) is the integral of the contributions from all upwind surface CO₂ emissions. The relative weight of each surface point source emission on F_{CO_2} depends on its location relative to the EC instrumentation. F_{CO_2} is related to the distribution of source CO₂ fluxes at the surface $(x', y', z' = z_0)$ with strength Q_{CO_2} by the footprint function or source weight function, $f(x_m - x', y_m - y', z_m - z_0)$:

$$F_{CO_2}(x_m, y_m, z_m) = \int_{-\infty}^{\infty} \int_{-\infty}^{\infty} Q_{CO_2}(x', y', z' = z_0) \cdot f(x_m - x', y_m - y', z_m - z_0) \cdot dx' \cdot dy' \quad (2)$$

(e.g., Horst and Weil, 1992; Schmid, 1997). The value of the footprint function generally rises to a maximum some distance upwind of the EC sensors, then smoothly falls off in all directions. The total surface influence on F_{CO_2} , or the source area, is the integral beneath the footprint function.

Similar to the methods of Werner et al. (2000; 2003), we compared EC with chamber measurements of CO₂ flux by modeling the footprint function for each half-hour EC measurement from 09/12/2006 to 09/21/2006. The Flux Source Area Model (FSAM) of Schmid (1997), based on analytic solutions of the advection-diffusion equation (Horst

and Weil, 1992) was used to model footprint functions using the following inputs: (1) z_m = 2.5 m; (2) surface roughness height, $z_0 = 0.03$ m, in accordance with Anderson and Farrar (2000); (3) measured mean horizontal wind direction; (4) cross-wind turbulence near the surface characterized by calculated σ_v/u_* , where σ_v is the standard deviation of the wind speed in the cross-wind direction; (5) calculated Monin-Obukhov length, L , if corresponded to unstable atmospheric conditions (i.e., only measurements corresponding to $L < 0$ were considered) (Table 1). We calculated f at the center of each 25-m² grid block in Figure 6. The source area was defined here as the area within which 90% of the measured EC flux was derived from. Results indicated that the source area was located within ~100 m upwind of the EC station for all of the 73 footprint functions modeled (mean = 86 m, range = 26 to 108 m; Figure 8). In other words, the source area was contained within the tree kill area for all modeled footprint functions.

On each day from 09/12/2006 to 09/21/2006, Q_{CO_2} was assumed equal to the chamber CO₂ flux in Figure 6. The product of Q_{CO_2} and f was then calculated for each 25-m² grid block and summed over the source area, yielding the “footprint CO₂ flux”. Figure 9 shows a histogram of the relative difference between the measured EC CO₂ flux and the footprint CO₂ flux, expressed as a percent of the EC flux. The mean relative difference was -0.3%, with a standard error = 2.7%. The standard deviation of the relative difference was 23% and the mode was offset positively from zero. No systematic relationship was observed between the relative difference and L , u_* , time of day, or wind direction for the ranges of values considered. A plot of EC versus footprint CO₂ flux (Figure 10a) shows that the data were moderately correlated ($R^2 = 0.42$ for 1:1 line). At

CO₂ flux up to ~1300 g m⁻² d⁻¹, the data clustered around the 1:1 line, while at higher flux, EC CO₂ fluxes tended to be biased high relative to footprint CO₂ fluxes. Mean vertical wind velocities (\bar{w}) corresponding to the modeled footprints ranged from -0.43 to 0.03 m s⁻¹ (mean and standard deviation = -0.17 and 0.12 m s⁻¹, respectively). \bar{w} was negatively correlated (correlation coefficient = -0.37) with the relative difference between the EC and footprint CO₂ fluxes, such that EC CO₂ fluxes were typically greater than footprint fluxes when \bar{w} was more negative.

The correlation of average daily EC and average daily footprint CO₂ flux increased substantially ($R^2 = 0.70$ for 1:1 line) relative to half-hour measurements, while the positive bias at flux >1300 g m⁻² d⁻¹ was reduced (Figure 10b). Furthermore, the correlation between average daily \bar{w} (Table 1) and the relative difference between EC and footprint CO₂ fluxes was reduced (correlation coefficient = 0.24) relative to half-hour measurements.

4.5. Relationships between temporal variations in EC CO₂ fluxes and meteorology

To assess the relationships between temporal variations in meteorological parameters and EC CO₂ fluxes, we calculated average daily EC CO₂ fluxes from 09/08/2006 to 10/24/2006 using fluxes corresponding to a narrow range of mean horizontal wind directions (250 to 290°; Figure 5b). Since the source area changes for each EC flux measurement depending on atmospheric conditions, a time series of EC fluxes is influenced by both temporal variations in, and spatial heterogeneity of, surface fluxes. This spatial component can complicate comparison of temporal variations in EC CO₂

fluxes to meteorological (or deep volcanic, hydrothermal) processes. Therefore, to limit the effects of spatial heterogeneity of surface fluxes on the evaluation of temporal variability of EC CO₂ fluxes, we only considered fluxes corresponding to a narrow range of mean horizontal wind directions (250 to 290°) in the calculation of average daily EC CO₂ fluxes (Figure 5b). However, in this simple analysis, it was not possible to assess changes in the same flux source area over time.

No systematic relationship was observed between average daily EC CO₂ flux and average daily atmospheric or soil temperature. A decrease in average daily and half-hour EC CO₂ fluxes was observed during precipitation events on 10/01/2007-10/02/2007 and 10/10/2007-10/11/2007 and in half-hour measurements on 10/17/2007 (Figures 5b and 7). Changes in EC flux associated with snowfall on 10/14/2007 were not possible to assess due to gaps in the time series of EC flux. From 09/08/2006 to 10/24/2006, average daily EC CO₂ flux was most strongly positively correlated with average daily atmospheric pressure (correlation coefficient = 0.52) and inversely correlated with average daily wind speed (correlation coefficient = -0.33) at one-day time lag (Figure 5a and b). From 09/08/2006 to 09/22/2006 (zone I, Figure 5a and b), average daily EC CO₂ flux was more strongly correlated with average daily wind speed (correlation coefficient = -0.70) than with average daily atmospheric pressure (correlation coefficient = 0.57). However, from 09/24/2006 to 10/10/2006 (zone II, Figure 5a and b), EC CO₂ flux was more strongly correlated with atmospheric pressure (correlation coefficient = 0.64) than with wind speed (correlation coefficient = -0.39).

4.6. Eddy covariance heat fluxes

Measured H from 09/08/2006 to 10/24/2006 ranged from -91.9 to 466 W m^{-2} , with a mean and standard deviation of 52.2 and 106.2 W m^{-2} , respectively. Measured LE ranged from -99.9 to 176.4 W m^{-2} , with a mean and standard deviation of 19.3 and 34.7 W m^{-2} , respectively.

Neglecting the heat stored in the air beneath the sensors and horizontal advection, the one-dimensional energy balance for the tree kill can be written as:

$$Rn - G = LE + H, \quad (3)$$

where Rn and G are the net radiation and heat flux into the soil, respectively. Their difference represents the available energy. Figure 11 shows $LE + H$ versus $Rn - G$ measured at the HLTK from 09/08/2006 to 10/24/2006. Data were categorized based on time of day using PAR measurements and atmospheric stability using the stability parameter ξ

$$\xi = \frac{z_m - d}{L} \quad (4)$$

(Garrat, 1992). d is the zero-plane displacement, estimated as 63% of canopy height, which we assumed to equal zero based on absence of a canopy within the much of the source areas. Measured turbulent heat fluxes were well correlated with available energy

($R^2 = 0.77$ for 1:1 line). We calculated the relative difference between $H + LE$ and $Rn - G$, expressed as percent of $H + LE$. Systematic energy imbalances were observed, depending on time of day and atmospheric stability. The mean relative difference for energy fluxes measured at night was 44.1%. For fluxes measured during the day during neutral and stable conditions ($\xi > -0.1$), the mean relative difference was -47.3%, whereas it was -34.8% for fluxes measured during unstable-daytime ($\xi \leq -0.1$) periods. No systematic relationships were observed between \bar{w} and the relative difference between $H + LE$ and $Rn - G$.

5. Discussion

5.1. Performance evaluation of eddy covariance

The average CO_2 flux ($1346 \text{ g m}^{-2} \text{ d}^{-1}$) measured by EC from 09/08/2006 to 10/24/2006 at the HLTK (Figure 7) fell within the range of average fluxes (691 to $1382 \text{ g m}^{-2} \text{ d}^{-1}$) measured by Anderson and Farrar (2001) during their three sampling campaigns in 1996-1998. While the general similarity of measured values is encouraging, direct comparison of the two studies is not possible due to the different flux source areas that were sampled in the two studies. For example, the EC stations in the Anderson and Farrar (2001) study were located north of our EC station (Figure 2); thus, portions of asphalt parking lot were likely located within their flux source areas. In addition, comparison of EC fluxes measured in the different studies will also be complicated by the large spatial-temporal

variations in surface CO₂ fluxes that occur within the tree kill on diurnal to inter-annual timescales (e.g., Gerlach et al., 1998; Rogie et al., 2001; Lewicki et al., 2007).

We used footprint modeling to compare EC to chamber measurements of CO₂ fluxes at the HLTK. With a mean relative difference of $-0.3 \pm 2.7\%$ between half-hour EC and footprint CO₂ fluxes (Figure 9), the measurements were on average nearly unbiased. At relatively high flux, half-hour EC CO₂ fluxes tended to be biased high, relative to footprint CO₂ fluxes. Also, datasets for the HLTK were moderately correlated (Figure 10a), with a variance in the relative difference of 23%. Table 2 shows relative differences between EC and chamber CO₂ fluxes in volcanic and hydrothermal systems. Using footprint models to compare chamber to EC CO₂ fluxes, the Werner et al. (2000; 2003) investigations are most analogous to this study. Our results for the HLTK were similar to those reported by Werner et al. (2003) for diffusely degassing areas of Solfatara volcano, Italy (Figure 10a; Table 2). On average, a larger relative difference was observed between EC and chamber CO₂ fluxes for the Yellowstone National Park data, likely due in part to the presence of hydrothermal features within the EC source areas (Werner et al., 2000). Also, a larger dataset would be required for Yellowstone for closer comparison with other studies. While Anderson and Farrar (2001) did not directly compare EC to chamber CO₂ fluxes at the HLTK based on footprint modeling, they reported relative differences between average EC CO₂ fluxes calculated for the duration of their pilot studies and average chamber CO₂ fluxes measured in independent studies. Based on this analysis, they reported significantly larger negative bias in EC relative to chamber flux measurements than reported in other studies (Table 2).

456
457 Several factors may account for the differences observed between half-hour EC and
458 footprint CO₂ fluxes (Figures 9 and 10a). First, both the EC method and the analytic
459 footprint model assume homogeneous surface fluxes, flat terrain, and uniform surface
460 roughness. However, systematic errors associated with violations to these assumptions
461 could be difficult to diagnose because they will depend on interactions between terrain,
462 wind direction and speed, and atmospheric stability. EC fluxes were on average
463 unbiased relative to footprint fluxes and no systematic relationship was observed when
464 comparing the relative difference between the EC and footprint CO₂ fluxes and the
465 ranges of L , u_* , time of day, or wind direction considered in the analysis. However, we
466 observed positive bias of EC relative to footprint CO₂ fluxes at relatively high flux. Also,
467 the relative difference between EC and footprint CO₂ fluxes increased as \bar{w} became
468 more negative. Non-zero \bar{w} values can be indicative of advective flux (e.g., Lee, 1998;
469 Turnipseed et al., 2003), but interpretations of their effect on EC fluxes vary. Lee (1998)
470 suggested that horizontal flow divergence below the EC measurement height caused
471 negative \bar{w} and loss of CO₂ flux at night under stable conditions over a deciduous forest.
472 However, over a coniferous forest in mountainous terrain, Turnipseed et al. (2003)
473 interpreted positive \bar{w} values and loss of CO₂ flux at night under stable stratification to
474 reflect flow convergence near the EC tower due to local changes in terrain. We only
475 deployed a single EC station, and so we cannot assess the horizontal advective fluxes
476 necessary to close the conservation of mass equations that would be required to
477 understand the sign and cause of the bias we observe. We suspect that the negative bias
478 in \bar{w} and positive bias in EC CO₂ flux at high flux we observe under unstable conditions

likely result from air flow changes as wind interacts with the complicated terrain of the study area. Presumably, a planar-fit coordinate rotation (Wilczak et al., 2001) could be used to reduce vertical-wind bias. Finally, the effects of wind drag on downhill horizontal flows would likely only subtly affect wind speed gradients, since standing dead wood within the EC source areas was sparsely distributed and free of foliage and fine branches. In fact, the observed negative bias in \overline{w} is opposite to what we might expect if wind drag slowed airflow and forced up-flow near the EC station.

Second, aspects of the chamber method can lead to underestimation or overestimation of soil CO₂ fluxes. For example, fluxes measured by vented chambers can be systematically high during windy times due to Venturi effects (e.g., Conen and Smith, 1998). While we cannot rule this effect out for all measurements, we did not find evidence for systematic overestimation of chamber CO₂ fluxes at the HLTK. In addition, some infiltration of atmospheric air into the chamber during windy periods could have occurred, biasing chamber CO₂ fluxes low. However, this effect would not account for the spatially systematic decrease in soil CO₂ flux that was observed on 09/14/2007 with high average daily wind speed, and then following the passage of the cold front on 09/16/2007 when low average daily wind speed was observed (Figure 6; Lewicki et al., 2007). Rather, we would expect wind-driven air infiltration into the chamber to affect chamber flux measurements randomly over the study area. Placement of the chamber on the soil surface disturbs the soil properties and gas flow during the time of measurement, which can lead to systematically low flux measurements when advective soil gas flow occurs (Welles et al., 2000; Evans et al., 2001). While we attempted to correct chamber

measurements for this effect prior to the footprint analysis, it is possible that chamber fluxes were under-corrected at relatively high flux, thus potentially contributing to the high EC relative to footprint CO₂ fluxes.

Third, we demonstrated that large variations occur in the spatial distribution and magnitude of surface CO₂ fluxes over relatively short periods of time within the tree kill area (Figure 6), which are difficult to characterize with the chamber method, even when measurements are repeated on a daily basis. As a result, our assumption that on any given day, over the entire day, the distribution of source CO₂ fluxes is equal to the measured chamber fluxes on that day probably introduced error into the comparison.

Finally, random errors associated with both the EC and chamber methods (e.g., Chiodini et al., 1998; Baldocchi, 2003) were likely important sources of variability in the comparison. Nonetheless, given all of the complexities of the HLTK site, it is encouraging that relatively small biases exist in our dataset, which reinforces our assertion that the EC method may be used with some success in such environments.

When the half-hour EC and footprint CO₂ fluxes were averaged over daily timescales, the correlation improved substantially (Figure 10b). Also, the positive bias observed at relatively high flux in half-hour EC relative to footprint CO₂ fluxes was reduced in the average daily fluxes. Since each grid of chamber measurements was typically completed over ~8 hours on a given day, averaging EC and footprint CO₂ fluxes over day-long periods allowed us to evaluate the measurements over more comparable timescales. This likely contributed to the improved correlation observed between average daily EC and

footprint CO₂ fluxes. Our results suggest that if monitoring variations in surface CO₂ fluxes over timescales longer than a day is adequate for the investigation of interest (e.g., volcano monitoring), then the EC technique can perform well under certain complex site conditions.

Average *H* and *LE* values measured from 09/08/2006 to 10/24/2006 fell within the range of average values measured by Anderson and Farrar (2001) during their three sampling campaigns at the HLTK. These values were lower than those measured by Werner et al. (2006) at Solfatara volcano, which is expected due to the relatively high soil temperatures and steam condensation in soils in the Solfatara hydrothermal area. Also, Werner et al. (2006) found that measurements of *H* and *LE* were positively correlated with EC CO₂ fluxes in the Solfatara hydrothermal area, reflecting a large volcanic component in all fluxes. We found no systematic relationship between these parameters at the HLTK, due to the different sources of heat (non-volcanic) and CO₂ (volcanic).

We further assessed the performance of EC at the HLTK by comparing EC heat flux measurements to measurements made by independent methods. While the degree of energy balance closure obtained in the field is directly applicable to evaluation of *H* and *LE*, its utility in the evaluation of CO₂ fluxes will depend on whether sources of error are associated with the EC method or in determining the available energy terms (e.g., Wilson et al., 2002). The degree of energy balance closure observed (Figure 11) fell within the range of that observed at FLUXNET sites, where energy fluxes were measured over a wide range of ecosystems and climates, typically with more ideal terrain and surface flux

characteristics than observed at the HLTK (Wilson et al., 2002). Turbulent heat fluxes at the tree kill were typically underestimated relative to available energy during daytime hours, whereas during nighttime hours, turbulent heat fluxes were overestimated relative to available energy.

Lack of complete energy balance closure can result from a range of issues, including systematic and random sampling errors, lack of complete estimation of heat stored beneath the EC sensors, inherent low and high pass filtering associated with the EC method, and advection of heat induced by horizontal heterogeneity of surface fluxes and complex terrain (e.g., Wilson et al., 2002). While it is not possible to unequivocally determine the sources of error and their relative importance in the energy balance assessment, one or more issues could be relevant to the HLTK area. First, the source areas sampled by the soil heat flux plates (cm^2 scale), net radiometer (m^2 scale), and EC vary between one another by up to several orders of magnitude. Therefore, variations in the surface conditions (e.g., slope geometry and sun facing angle, presence of rocks and standing/fallen deadwood) and climate within the different source areas likely induced systematic biases in the energy balance calculation. Second, while the poorer energy balance closure observed during neutral-and-stable-daytime relative to unstable-daytime periods could be due in part to heat storage in the air beneath the EC sensors, this effect was unlikely to be substantial because of the short height of the EC system and either near-absence of a canopy in the EC system source areas. Third, advection associated with wind speed gradients could, in principal, bias EC heat fluxes similarly to CO_2 . Since we observed (1) no systematic relationship between \overline{w} and the relative difference

between $H + LE$ and $Rn - G$ and (2) substantially greater bias in EC heat flux versus available energy measurements than in EC versus footprint CO_2 fluxes, it is likely that the role of advection is minor relative to other factors such as difference in source area in the lack of energy balance closure at the HLTK.

5.2. Influence of meteorological forcing on surface CO_2 fluxes

Lewicki et al. (2007) showed that large spatio-temporal variations in surface CO_2 fluxes measured by the chamber method at the HLTK from 09/12/2006 to 09/21/2006 were meteorologically driven. They calculated total CO_2 discharge rates for the study area based on chamber measurements and found them to be positively correlated with average daily atmospheric pressure and inversely correlated with average daily wind speed, most strongly at one-day time lag. While the processes driving these relationships likely involved complex interactions between meteorology, topography, and vadose zone gas flow, Lewicki et al. (2007) suggested that spatio-temporal changes in surface CO_2 fluxes may have been primarily due to dynamic coupling between the flow of volcanic CO_2 at depth within the vadose zone and wind.

Despite the complications introduced into the EC CO_2 flux time series by the temporally varying flux source area, we observed similar relationships between average daily EC CO_2 fluxes and average daily wind speed and atmospheric pressure from 09/08/2006 to 09/22/2006 (zone I, Figure 5a and b) to those observed by Lewicki et al. (2007) for chamber measurements over a similar time period. The relatively high degree of

correlation observed between average daily EC CO₂ flux and wind speed from 09/08/2006 to 09/22/2006 was likely due to the cold front that passed through the region during that time bringing high winds that could have modulated vadose zone gas flow (Lewicki et al., 2007). However, from 09/24/2006 to 10/10/2006 (zone II, Figure 5), EC CO₂ flux was more strongly correlated with atmospheric pressure and more weakly correlated with wind speed. This was probably due to the lower magnitude variations in average daily wind speed over this time period having less influence on subsurface gas flow to the atmosphere. Overall, our results indicate that similar to the chamber method, EC can be used to monitor background changes in volcanic CO₂ fluxes driven by meteorological forcing, and presumably changes related to deeply derived processes such as volcanic activity.

It is likely that precipitation events, and associated increases in soil moisture content also affected surface CO₂ fluxes at the HLTK. However, it was only possible to assess the relationship between EC CO₂ fluxes and precipitation in a limited fashion due to gaps in the time series of EC flux caused by data filtering for wind direction, u_* , and stationarity. This emphasizes the issue that potentially large gaps in time series of EC flux data must be tolerated, particularly at a site such as the HLTK. For example, we lost about half of the half-hour EC CO₂ flux data for the given wind direction range of interest (190 to 360°) due to insufficient turbulence and non-stationarity in the data. Automated and continuous chamber measurements at a fixed location within the study area (e.g., Rogie et al., 2001; Werner et al., 2003) would be valuable to supplement EC data.

6. Summary and Conclusions

We measured a six-week time series of EC CO₂ and heat fluxes at the HLTK on Mammoth Mountain, a site with heterogeneous distribution of source fluxes and complex terrain that challenged the underlying assumptions of EC theory.

1. Half-hour EC CO₂ fluxes were compared with chamber fluxes measured repeatedly on a daily basis using footprint modeling. EC CO₂ fluxes were moderately correlated with, and on average unbiased relative to, footprint CO₂ fluxes. The average relative difference between HLTK EC and footprint CO₂ fluxes was similar to that reported for diffusely degassing areas at Solfatara volcano, Italy (Werner et al., 2003). Even though HLTK chamber CO₂ fluxes were measured on a daily basis, it was not possible to completely characterize spatio-temporal variations in source CO₂ fluxes on the time scale of the EC measurements. This factor, as well as advection of CO₂ due to topographic variations and the inherent random errors associated with both the EC and chamber methods likely contributed to the differences observed between CO₂ fluxes measured by the two techniques.

2. Average daily EC CO₂ fluxes were well correlated with average daily footprint CO₂ fluxes, indicating that when random error is reduced in CO₂ flux measurements by temporal averaging, the EC technique can perform well under certain complex site conditions. However, potential volcanic and geothermal sites for deployment of EC must be evaluated on an individual basis to assess viability of the method.

640

641 3. Turbulent heat fluxes were well correlated with available energy at the HLTK and the
642 degree of energy balance closure fell within the range observed in many investigations
643 conducted in contrasting ecosystems and climates with more ideal terrain and surface flux
644 characteristics.

645

646 4. Average daily EC CO₂ fluxes were correlated with both average daily wind speed and
647 atmospheric pressure over the observation period, the degree to which depended on the
648 magnitude of the fluctuations in the atmospheric parameters. The relationships between
649 EC CO₂ fluxes and wind speed and atmospheric pressure were similar to those observed
650 between chamber CO₂ fluxes and the atmospheric parameters over a comparable time
651 period. Similar to the chamber method, EC can be used to monitor background changes
652 in volcanic CO₂ fluxes driven by meteorological forcing, and presumably changes related
653 to deeply derived processes such as volcanic activity.

654

655 5. EC provides the benefit over the chamber method of a time and space-averaged
656 measurement of surface CO₂ flux that is essentially fully automated. However,
657 potentially large gaps in time series of data must be tolerated with EC, depending on site
658 characteristics and atmospheric conditions. Also, the spatial distribution of surface CO₂
659 fluxes cannot be mapped in detail by EC, as it can by the chamber method. The chamber
660 and EC methods are therefore best used together, providing complementary information
661 in volcanic gas surveillance programs.

662

Acknowledgements

We thank C. Werner, an anonymous reviewer, and S. Biraud for comments that greatly improved the manuscript, T. Tosha and R. Aoyagi for assistance in the field, and H.P. Schmidt for the FSAM source code. This work was supported by the Ministry of Economy, Trade, and Industry (METI) of Japan through the Lawrence Berkeley National Laboratory Sponsored Project Office Contract No. LB06002281, and by the Zero Emissions Research and Technology (ZERT) project, supported by the Assistant Secretary for Fossil Energy, Office of Sequestration, Hydrogen, and Clean Coal Fuels, through the National Energy Technology Laboratory, U.S. Department of Energy, under Contract No. DE-AC02-05CH11231.

References

- Anderson, D.E., Farrar, C.D., 2001. Eddy covariance measurement of CO₂ flux to the atmosphere from an area of high volcanogenic emissions, Mammoth Mountain, California. *Chemical Geology*, 177, 31–42.
- Aubinet, M., Grelle, A., Ibrom, A., et al., 2000. Estimates of the annual net carbon and water exchange of European forests: the EUROFLUX methodology. *Advances in Ecological Research*, 30, 113–175.
- Bailey, R.A., 1989. Geologic map of the Long Valley Caldera, Mono-Inyo Craters volcanic chain and vicinity, eastern California, scale 1:62,500. U.S. Geological Survey Miscellaneous Investigations Map, I-1933.
- Baldocchi, D.D., 2003. Assessing the eddy covariance technique for evaluating carbon dioxide exchange rates of ecosystems: past, present, and future. *Global Change Biology*, 9, 479–492.
- Baldocchi, D.D., Hicks, B.B., Meyers, T.P., 1988. Measuring biosphere-atmosphere exchanges of biologically related gases with micrometeorological methods. *Ecology*, 69, 1331–1340.
- Baubron, J.-C., Allard, P., Sabroux, J.-C., Tedesco, D., Toutain, J.P., 1991. Soil gas emanations as precursory indicators of volcanic eruptions. *Journal of the Geological Society*, 148, 571–576.
- Bergfeld, D., Goff, F., Janik, C.J., 2001. Elevated carbon dioxide flux at the Dixie Valley geothermal field, Nevada; relations between surface phenomena and the geothermal reservoir. *Chemical Geology*, 177, 43–66.

697 Billesbach, D.P., Fischer, M.L., Torn, M.S., Berry, J.A., 2004. A portable eddy
 698 covariance system for the measurement of ecosystem-atmosphere exchange of
 699 CO₂, water vapor, and energy. *Journal of Atmospheric and Oceanic Technology*
 700 21, 639–650.

701 Chiodini, G., Cioni, G. R., Guidi, M., Raco, B., Marini, L., 1998. Soil CO₂ flux
 702 measurements in volcanic and geothermal areas. *Applied Geochemistry*, 13, 543–
 703 552.

704 Conen, F., Smith, K.A., 1998. A re-examination of closed flux chamber methods for the
 705 measurement of trace gas emissions from soils to the atmosphere. *European*
 706 *Journal of Soil Science*, 49, 701-707.

707 Connor, C.B., Clement, B.M., Song, X.D., Lane, S.B., Westthomas, K., 1993.
 708 Continuous monitoring of high-temperature fumaroles on an active lava dome,
 709 Volcan Colima, Mexico- Evidence of mass-flow variation in response to
 710 atmospheric forcing. *Journal of Geophysical Research*, 98, 19,713–19,722.

711 Evans, W. C., Sorey, M. L., Kennedy, B. M., Stonestrom, D. A., Rogie, J. D., Shuster,
 712 D.L., 2001. High CO₂ emissions through porous media: Transport mechanisms
 713 and implications for flux measurement and fractionation. *Chemical Geology*, 177,
 714 15–29.

715 Farrar, C.D., Sorey, M.L., Evans, W.C., Howle, J.F., Kerr, B.D., Kennedy, B.M., King,
 716 Y., Southon, J.R., 1995. Forest-killing diffuse CO₂ emission at Mammoth
 717 Mountain as a sign of magmatic unrest. *Nature*, 376, 675–678.

718 Farrar, C.D., Neil, J.M., Howle, J.F., 1998. Magmatic carbon dioxide emissions at
719 Mammoth Mountain, California. U.S. Geological Survey Water Resources
720 Investigation Report 98-4217, 34 pp.

721 Folken, Th., Wichura, B., 1996. Tools for quality assessment of surface-based flux
722 measurements. *Agricultural and Forest Meteorology*, 78, 83–105.

723 Garrat, 1992. *The Atmospheric Boundary Layer*. Cambridge University Press,
724 Cambridge, 316 p.

725 Gerlach, T.M., Doukas, M.P., McGee, K.A., Kessler, R., 1998. Three-year decline of
726 magmatic CO₂ emissions from soils of a Mammoth Mountain tree kill: Horseshoe
727 Lake, CA, 1995-1997. *Geophysical Research Letters*, 25, 1947–1950.

728 Gerlach, T.M., Doukas, M.P., McGee, K.A., Kessler, R., 2001. Soil efflux and total
729 emission rates of magmatic CO₂ at the Horseshoe Lake tree kill, Mammoth
730 Mountain, California, 1995-1999. *Chemical Geology*, 177, 101–116.

731 Granieri, D., Chiodini, G., Marzocchi, W., Avino, R., 2003. Continuous monitoring of
732 CO₂ soil diffuse degassing at Phlegrean Fields (Italy): influence of environmental
733 and volcanic parameters. *Earth and Planetary Science Letters*, 212, 167–179.

734 Hernandez, P.A., Perez, N., Salazar, J.M., Nakai, S., Notsu, K., Wakita, H., 1998.
735 Diffuse emissions of carbon dioxide, methane, and helium-3 from Teide volcano,
736 Tenerife, Canary Islands. *Geophysical Research Letters*, 25, 3311–3314.

737 Hernandez, P.A., Notsu, K., Salazar, J.M., Mori, T., Natale, G., Okada, H., Virgilli, G.,
738 Shimoike, Y., Sato, M., Perez, N.M., 2001. Carbon dioxide degassing by
739 advective flow from Usu volcano, Japan. *Science*, 2001, 83–86.

740 Hill, D.P., 1996. Earthquakes and carbon dioxide beneath Mammoth Mountain,
741 California. *Seismological Research Letters*, 67, 8–15.

742 Hill, D.P., Prejean, S.G., 2005. Volcanic unrest beneath Mammoth Mountain, California.
743 *Journal of Volcanology and Geothermal Research*, 146, 257–283.

744 Horst, T.W., Weil, J.C., 1992. Footprint estimation for scalar flux measurements in the
745 atmospheric surface-layer. *Boundary-Layer Meteorology*, 59, 279-296.

746 Kaimal, J.C., Finnigan, J.J., 1994. *Atmospheric Boundary Layer Flows: Their Structure*
747 *and Measurement*. Oxford University Press, Oxford.

748 Klusman, R.W., Moore, J.N., LeRoy, M.P., 2000. Potential for surface gas
749 measurements in exploration and surface evaluation of geothermal resources.
750 *Geothermics*, 29, 637–670.

751 Lee, X., 1998. On micrometeorological observations of surface-air exchange above tall
752 vegetation. *Agricultural and Forest Meteorology*, 91, 39-49.

753 Lewicki, J.L., Bergfeld, D., Cardellini, C., Chiodini, G., Granieri, D., Varley, Werner, C.,
754 2005. Comparative soil CO₂ flux measurements and geostatistical estimation
755 methods on Masaya volcano. Nicaragua, *Bulletin of Volcanology*, 68, 76-90, doi:
756 10.1007/s00445-005-0423-9.

757 Lewicki, J.L., Hilley, G.E., Tosha, T., Aoyagi, R., Yamamoto, K., Benson, S.M., 2007.
758 Dynamic coupling of volcanic CO₂ flow and wind at the Horseshoe Lake tree kill,
759 Mammoth Mountain, California. *Geophysical Research Letters*, 34, L03401,
760 doi:10.1029/2006GL028848.

761 McGee, K.A., Gerlach, T.M., 1998. Annual cycle of magmatic CO₂ in a tree-kill soil at
762 Mammoth Mountain, California: Implications for soil acidification. *Geology*, 26,
763 463–466.

764 McGee, K.A., Gerlach, T.M., Kessler, R., Doukas, M.P., 2000. Geochemical evidence for
765 a magmatic CO₂ degassing event at Mammoth Mountain, California, September-
766 December 1997. *Journal of Geophysical Research*, 105, 8447–8456.

767 Rahn, T.A., Fessenden, J.E., Wahlen, M., 1996. Flux chamber measurements of
768 anomalous CO₂ emission from the flanks of Mammoth Mountain, California.
769 *Geophysical Research Letters*, 23, 1861–1864.

770 Rogie, J.D., Kerrick, D.M., Sorey, M.L., Chiodini, G., Galloway, D.L., 2001. Dynamics
771 of carbon dioxide emission at Mammoth Mountain, California. *Earth and*
772 *Planetary Science Letters*, 188, 535–541.

773 Schmid, H.P., 1997. Experimental design for flux measurements: matching scales of
774 observations and fluxes. *Agricultural and Forest Meteorology*, 87, 179–200.

775 Turnipseed, A.A., Anderson, D.E., Blanken, P.D., Baugh, W.M., Monson, R.K., 2003.
776 Airflows and turbulent flux measurements in mountainous terrain Part 1. Canopy
777 and local effects. *Agricultural and Forest Meteorology*, 119, 1–21.

778 Turnipseed, A.A., Anderson, D.E., Burns, S., Blanken, P.D., Monson, R.K., 2004.
779 Airflows and turbulent flux measurements in mountainous terrain Part 2.
780 Mesoscale effects. *Agricultural and Forest Meteorology*, 125, 187–205.

781 Webb, E.K., Pearman, G.I., Leuning, R., 1980. Correction of flux measurements for
782 density effects due to heat and water vapour transfer, *Quarterly Journal of Royal*
783 *Meteorological Society*, 106, 85–100.

784 Welles, J.M., Demetriades-Shah, T.H., McDermitt, D.K., 2000. Considerations for
785 measuring ground CO₂ effluxes with chambers. *Chemical Geology*, 177, 3-13.

786 Werner, C., Cardellini, C., 2006. Comparison of carbon dioxide emissions with fluid
787 upflow, chemistry, and geologic structures at the Rotorua geothermal system,
788 New Zealand. *Geothermics*, 35, 221–238.

789 Werner, C., Wyngaard, J.C., Brantley, S.L., 2000. Eddy-correlation measurement of
790 hydrothermal gases. *Geophysical Research Letters*, 27, 2925–2928.

791 Werner, C., Chiodini, G., Voigt, D., Caliro, S., Avino, R., Russo, M., Brombach, T.,
792 Wyngaard, J., Brantley, S., 2003. Monitoring volcanic hazard using eddy
793 covariance at Solfatara volcano, Naples, Italy. *Earth and Planetary Science*
794 *Letters*, 210, 561–577.

795 Werner, C., Chiodini, G., Granieri, D., Caliro, S., Avino, R., Russo, M., 2006. Eddy
796 covariance measurements of hydrothermal heat flux at Solfatara volcano, Italy.
797 *Earth and Planetary Science Letters*, 244, 72–82.

798 Wilczak, J.M., Oncley, S.P., Stage, S.A., 2001. Sonic anemometer tilt correction
799 algorithms. *Boundary Layer Meteorology*, 99, 127-150.

800 Wilson, K., Goldstein, A., Falge, E., Aubinet, M., Baldocchi, D., Berbigier, P.,
801 Bernhofer, C., Ceulemans, R., Dolman, H., Field, C., Grelle, A., Ibrom, A., Law,
802 B.E., Kowalski, A., Meyers, T., Moncrieff, J., Monson, R., Oechel, W.,
803 Tenhunen, J., Valentini, R., Verma, S., 2002. Energy balance closure at
804 FLUXNET sites. *Agricultural and Forest Meteorology*, 113, 223–243.

805

Figure Captions

Figure 1. View of the Horseshoe Lake tree kill located on the southeastern flank of Mammoth Mountain, adjacent to Horseshoe Lake. Red square shows approximate location of EC station.

Figure 2. Digital elevation model of the HLTK study area, outlined by white line (modified from Lewicki et al., 2007). White dots show locations of the chamber CO₂ flux measurement points. Red and yellow squares show approximate locations of EC stations in the present and Anderson and Farrar (2001) studies, respectively.

Figure 3. Plot of EC CO₂ flux versus friction velocity (u_*). Solid line is running average of EC CO₂ flux over a $0.1 \text{ m s}^{-1} u_*$ window. Vertical dashed line shows $u_* = 0.25 \text{ m s}^{-1}$.

Figure 4. Wind rose showing joint frequency distribution of mean horizontal wind speed and direction (half-hour averages) from 09/08/2006 to 10/24/2006, constructed using Frequency Works.

Figure 5. (a) Time series of average daily atmospheric pressure (stars) and wind speed (dots). (b) Time series of average daily EC CO₂ flux corresponding to wind directions from 250 to 290°. Symbols indicate number of measurements (n) used to calculate average daily EC CO₂ fluxes. Error bars are standard error of mean. Average daily EC CO₂ fluxes are missing on days where filtering has entirely eliminated half-hour data. Diamonds are average of chamber CO₂ fluxes measured repeatedly on daily basis over entire grid area grid from 09/12/2006 to

828 09/21/2006. Dark gray zones in indicate approximate timing of precipitation
829 events. See text for explanations of light grayed zones I and II.

830 Figure 6 (a-i). Time series (09/12/2006 to 09/21/2006) of maps of log chamber CO₂ flux.
831 White squares denote approximate location of EC station.

832 Figure 7. Time series of EC CO₂ flux corresponding to mean wind direction between 190
833 and 360°, $u_* > 0.25 \text{ m s}^{-1}$, and stationary measurements. Gray zones indicate
834 approximate timing of precipitation events.

835 Figure 8. Source areas (area within which 90% of the measured EC flux was derived
836 from) for 73 modeled footprints. Square shows location of EC station.

837 Figure 9. Histogram of the relative difference between EC and footprint CO₂ fluxes,
838 expressed as percent of EC flux.

839 Figure 10. Plots of (a) EC CO₂ flux versus footprint CO₂ flux for half-hour EC
840 measurements and (b) average daily EC CO₂ flux versus average daily footprint
841 CO₂ flux. Error bars show standard error of mean. Gray area encompasses data
842 from diffusely degassing areas at Solfatara volcano, Italy (Location 1; Werner et
843 al., 2003).

844 Figure 11. Plot of sum of latent (LE) and sensible (H) heat flux measured by EC versus
845 difference between net radiation (R_n) and soil heat flux (G) measured by
846 radiometer and heat flux plates, respectively from 09/12/2006 to 09/21/2006. Red
847 dots are measurements made during the nighttime. Black dots and squares are
848 measurements made during neutral-and-stable-daytime ($\xi > -0.1$) and unstable-
849 daytime ($\xi \leq -0.1$) periods. 1:1 line is shown.

850
851

Table 1. Daily averages of half-hour data used for EC-footprint CO₂ flux comparisons and mean vertical wind speed.

Date	<i>n</i>	EC CO ₂ flux (g m ⁻² d ⁻¹)	Footprint CO ₂ flux (g m ⁻² d ⁻¹)	<i>L</i> (m)	<i>u</i> _* (m s ⁻¹)	<i>σ</i> _v (m s ⁻¹)	Wind dir. (°)	\overline{w} (m s ⁻¹)
09/12/2006	3	1437.3	1327.9	-63.7	0.32	1.4	263	-0.05
09/13/2006	5	1252.2	1134.5	-62.5	0.32	1.4	225	0.03e ⁻¹
09/14/2006	23	856.8	1006.0	-1415.3	0.88	3.0	263	-0.26
09/18/2006	7	1032.4	1163.1	-76.9	0.37	1.5	236	-0.06
09/19/2006	14	1059.3	1061.4	-491.2	0.82	2.7	265	-0.25
09/20/2006	7	964.1	1060.5	-40.2	0.32	1.6	268	-0.09
09/21/2006	14	1436.4	1425.2	-60.4	0.51	1.9	262	-0.13

Table 2. Relative differences for EC and chamber CO₂ flux comparisons in volcanic and hydrothermal systems.

Site	Mean ± standard deviation relative difference between EC and chamber CO ₂ fluxes	n	Reference
Yellowstone National Park, USA	-4.1 ± 68 %	6	Werner et al. (2000)
Solfatara volcano, Italy	-0.4 ± 32%	66	Werner et al. (2003)
Mammoth Mountain, USA	-19 to -40 %	2	Anderson and Farrar (2001)
Mammoth Mountain, USA	-0.3 ± 23%	73	Present study

For Werner et al. (2000; 2003) and the present study, the relative difference is defined as the half-hour EC CO₂ flux minus footprint CO₂ flux, expressed as per-cent EC CO₂ flux.

The mean and standard deviation of these values are reported. For Anderson and Farrar (2001), the relative difference is the mean EC CO₂ flux for study duration (two pilot studies were considered) minus the mean chamber CO₂ flux measured in independent studies, expressed as per-cent mean EC CO₂ flux. Only the range of these values is reported.

Figures.



Figure 1.

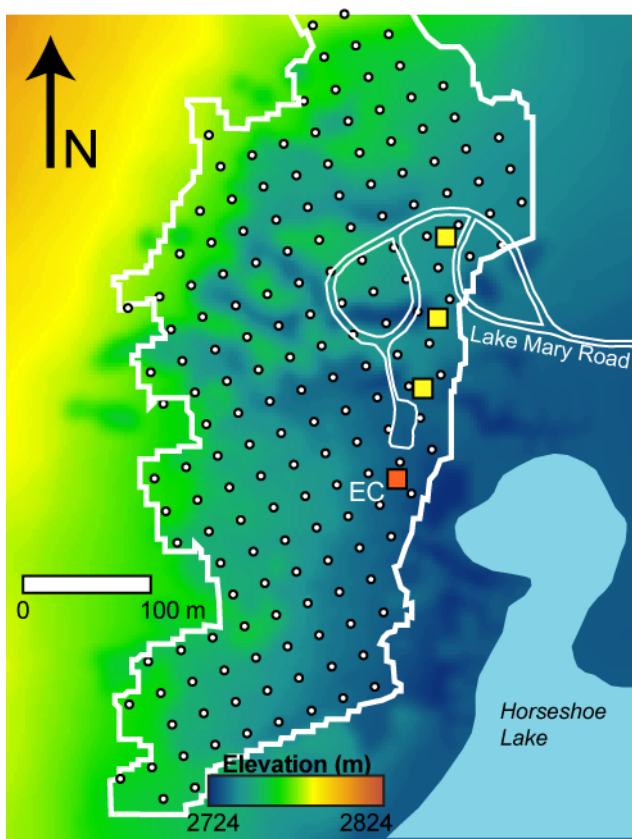


Figure 2.

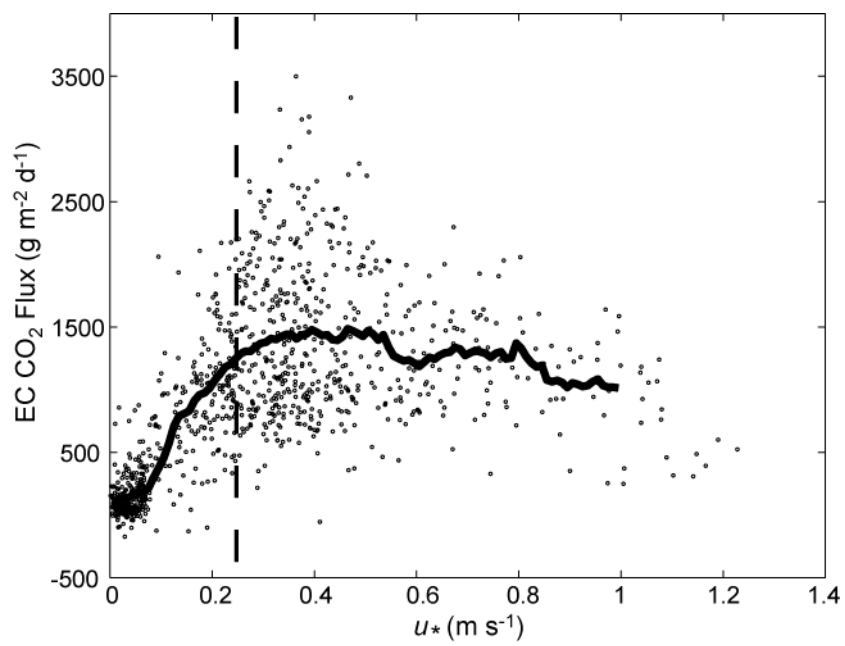


Figure 3.

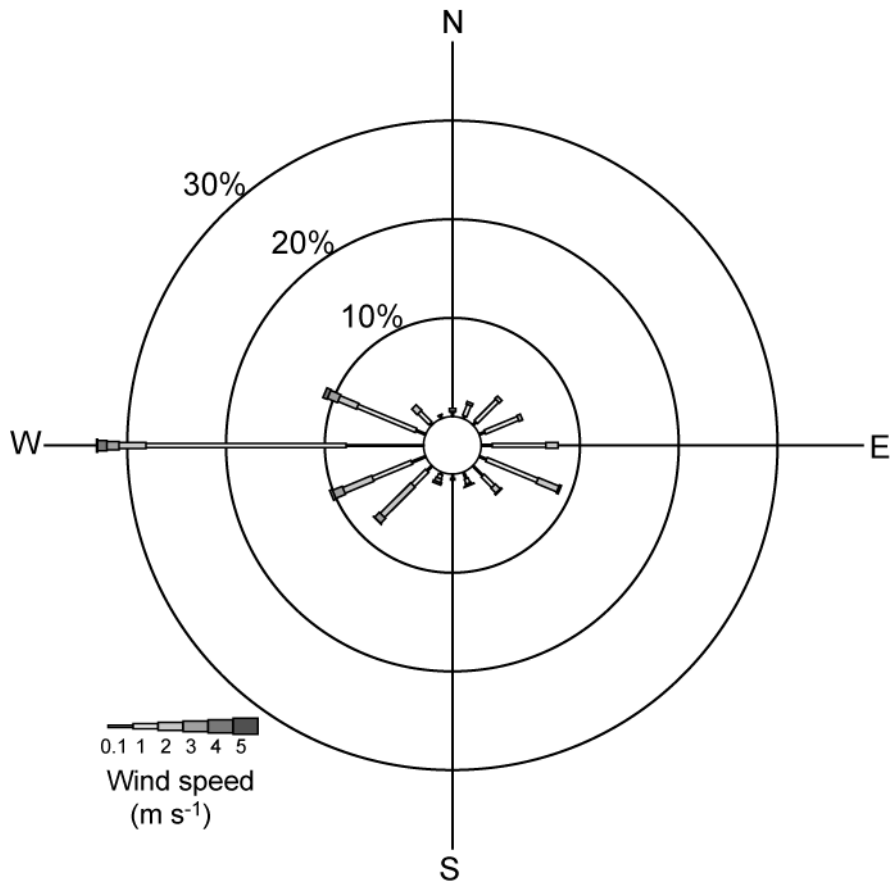


Figure 4.

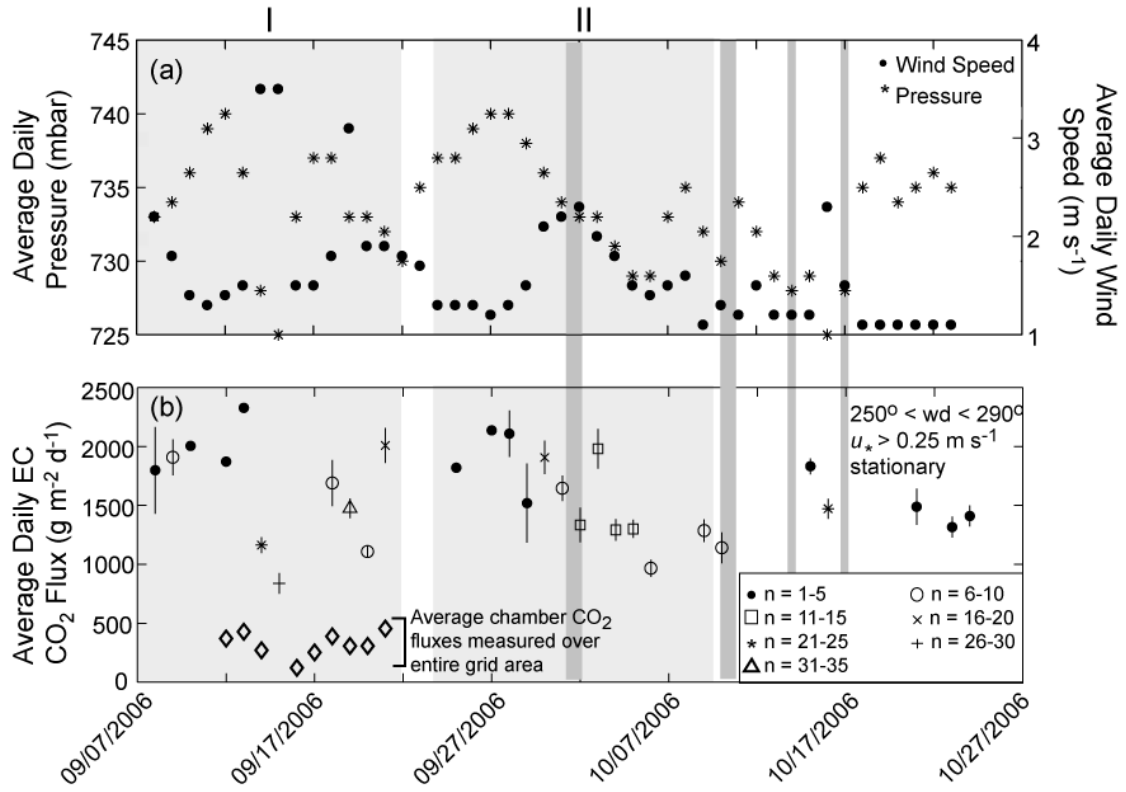


Figure 5.

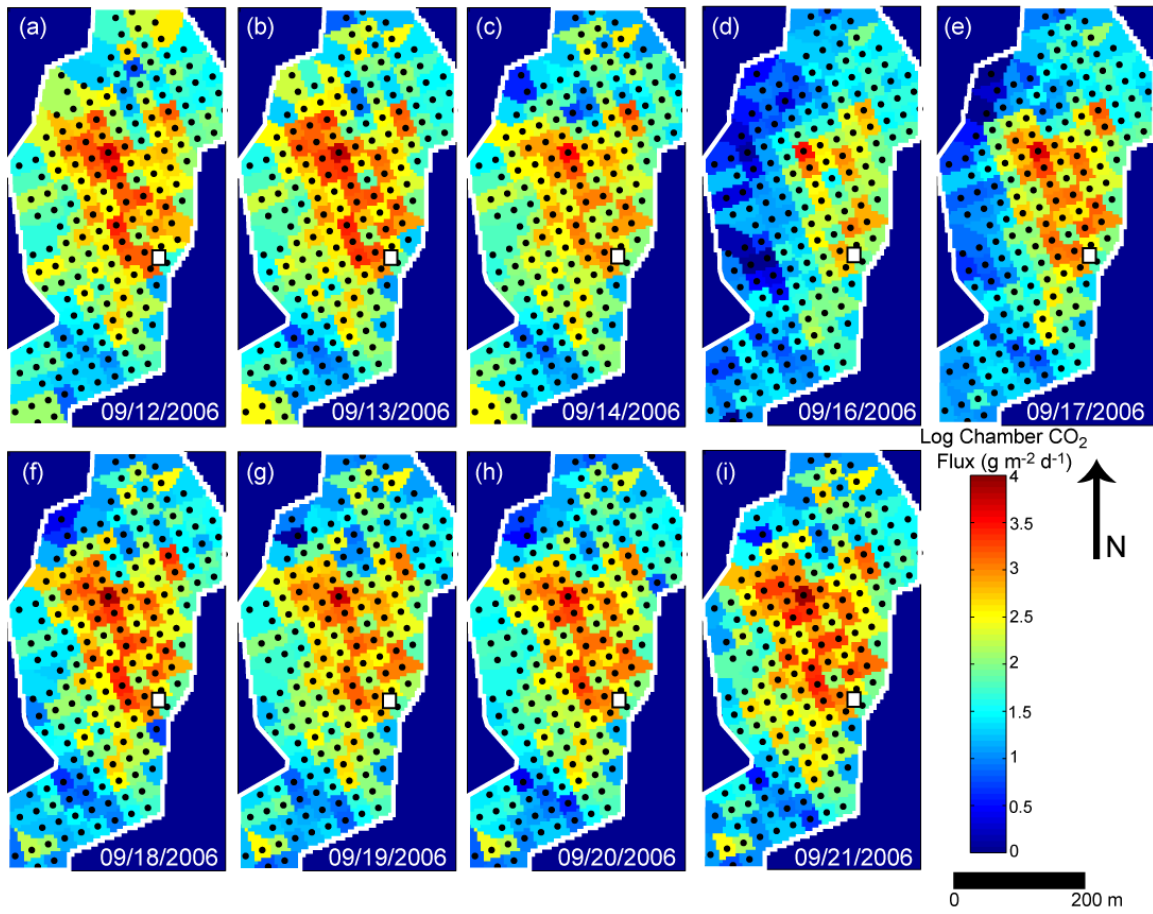


Figure 6.

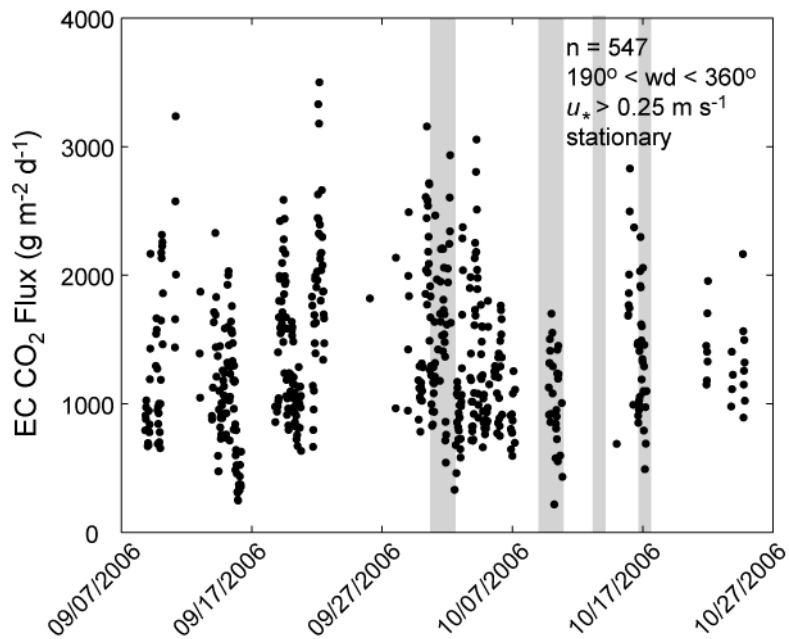
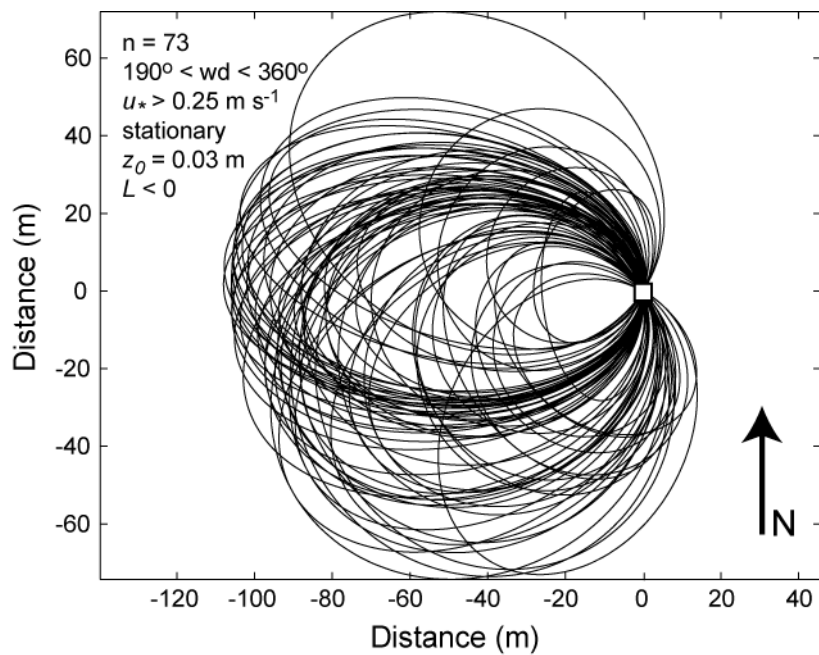


Figure 7.

887

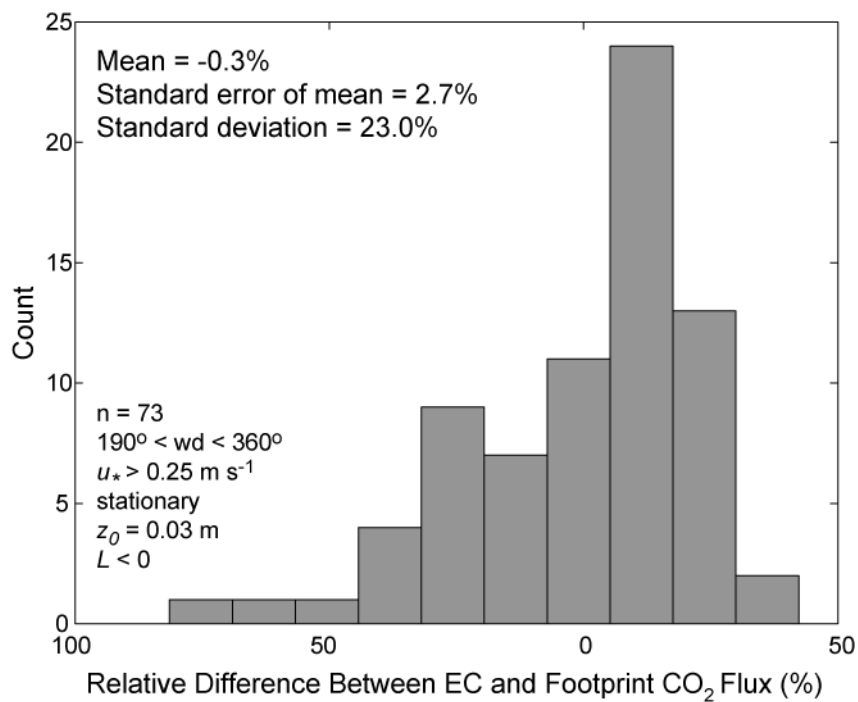


888

889

890

Figure 8.



891

892

893

Figure 9.

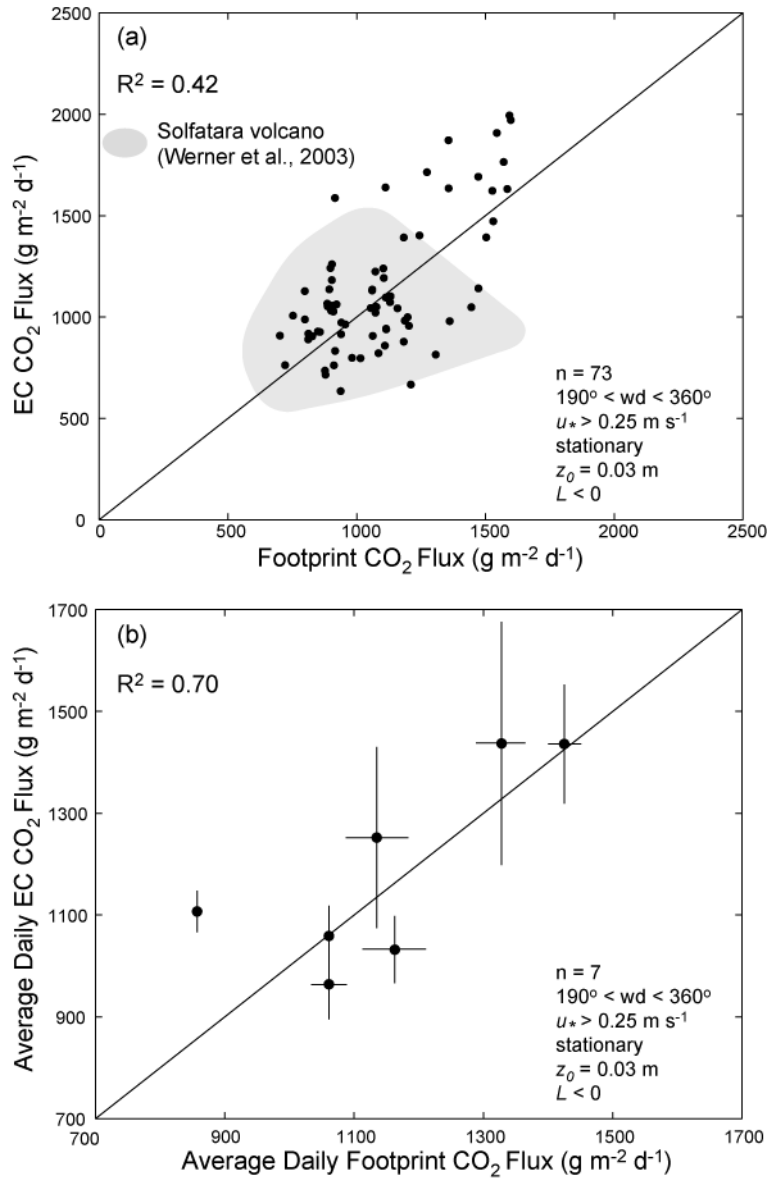


Figure 10.

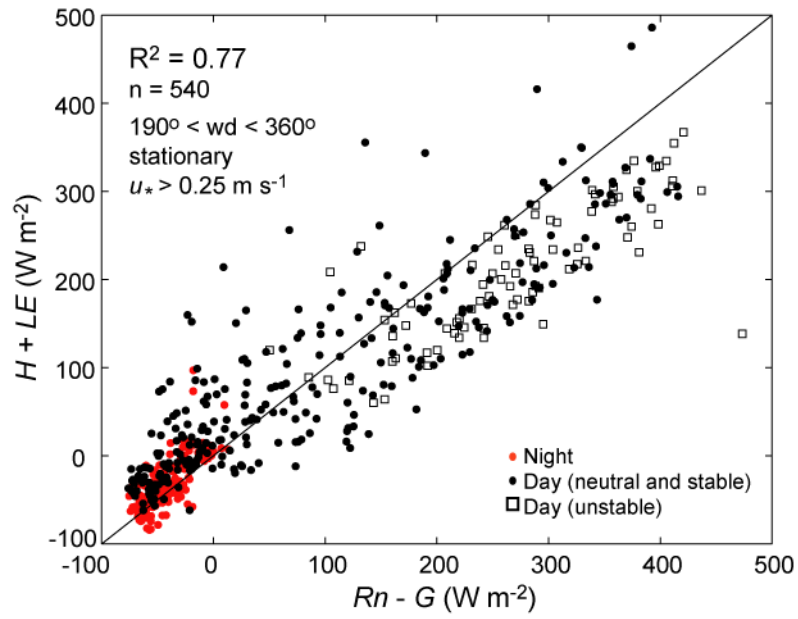


Figure 11.